Supplemental information to manuscript:

Suppression of new particle formation from monoterpene oxidation by NO_x

J. Wildt, Th. F. Mentel, A. Kiendler-Scharr, Th. Hoffmann, S. Andres, M. Ehn, E. Kleist, P. Müsgen, F. Rohrer, Y. Rudich, M. Springer, R. Tillmann, A. Wahner

This supplement is divided into 7 sections. In section S1 an overview on our treatment of the photochemical system is given. Section S2 describes the way to determine $P(O_3)$. Section S3 gives more details on power law dependencies mentioned in the manuscript. Section S4 describes determination of $[RO_2]$ from deviation of $\frac{[NO_2]}{[NO]}$ from PSS and section S5 gives details on our estimations of relative peroxy radical concentrations at low $[NO_x]_0$ conditions. Section S6 aims to confirm that the formation of first generation permutation reaction products is not the rate limiting step for new particle formation. Section S7 gives information on our determinations of J_7 and its uncertainties.

S1. Basic reactions and considerations regarding the power law dependence observed between ozone production rates and new particle formation

In the absence of volatile organic compounds (VOC) and hydroxyl radicals (OH), nitrogen monoxide (NO), nitrogen dioxide (NO_2), and ozone (O_3) reach equilibrium concentrations within minutes in a photochemical system. The equilibrium conditions are termed as photostationary steady state (PSS, Leighton, 1961):

$$\frac{[NO_2]}{[NO]} = \frac{k_1 \cdot [O_3]}{J(NO_2)} \qquad \text{(ES1)}$$

($k_1 = 1.8 \times 10^{-14}$ cm^3 s^{-1} = rate constant for the reaction of NO with O_3, IUPAC, 2009, $J(NO_2)$ = NO_2 photolysis rate).

The ratio $\frac{[NO_2]}{[NO]}$ deviates from that in Equation ES1 when the chemical system contains VOC and OH. This deviation from PSS is due to reactions of NO with peroxy radicals (RO_2). Reactions of NO with RO_2 either form NO_2 in reaction R2a or organic nitrates in reaction R2b:

$NO + RO_2 \rightarrow RO + NO_2$ (R2a)

$NO + RO_2 \rightarrow RONO_2$ (R2b)

Reaction R2a is the basic reaction for photochemical ozone formation. The rate of net ozone formation ($P(O_3)$) is written as:

$$P(O_3) = \sum_i([RO_2^i] \cdot k^i \cdot Y^i(O_3)) \cdot [NO] \quad \text{(ES2)}$$

In Equation ES2, RO_2^i is the specific peroxy radical, k^i the rate coefficient of RO_2^i with NO, and $Y^i(O_3)$ is the branching ratio of ozone formation in reaction R2 (reaction R2 = reaction R2a + reaction R2b) with the specific peroxy radical RO_2^i. The production rate of organic nitrate formation ($P(RONO_2)$) is given by:

$$P(RONO_2) = \sum_i([RO_2^i] \cdot k^i \cdot Y^i(RONO_2)) \cdot [NO] \quad \text{(ES3)}$$

In Equation ES3 $Y^i(RONO_2)$ is the branching ratio of organic nitrate formation in reaction R2.

For simplification we write Equations ES2 and ES3 in the form:

$$P(O_3) = k_2 \cdot [NO] \cdot [RO_2] \cdot Y(O_3) \quad \text{(ES2)}$$

and

$$P(RONO_2) = k_2 \cdot [NO] \cdot [RO_2] \cdot Y(RONO_2) \quad \text{(ES3)}$$

k_2 ($= k_{2a} + k_{2b}$) is an average rate constant for reaction R2 (9×10^{-12} cm^3 s^{-1}, IUPAC, 2009) and $Y(O_3)$ and $Y(RONO_2)$ are average branching ratios. Assuming that reactions R2a and R2b are the only pathways of RO_2 + NO reactions, $Y(RONO_2) = 1 - Y(O_3)$.

While reaction R2 is the dominant RO_2 loss at high NO_x conditions, reaction R3 (reaction R3 = reaction R3a + reaction R3b) is the main loss for RO_2 radicals at low NO_x conditions.

$RO_2 + HO_2 \rightarrow ROOH + O_2$ (R3a)

$RO_2 + R'O_2 \rightarrow$ Alkoxy radicals, diols, alkylperoxides (R3b)

Reaction R3a forms hydroperoxides. Reaction R3b forms various products including alkoxy radicals, diols, ketones (e.g. master chemical mechanism, MCM), and probably also alkylperoxides (e.g. Hallquist et al., 2009). We termed the sum of all products of reaction R3 as permutation reaction products, RPR. Production rates of PRP, P(PRP) can be written as:

$$P(PRP) = k_3 \cdot [RO_2] \cdot [RO_2] \quad \text{(ES4)}$$

where k_3 is an average rate constant for a given RO_2 mix. Note that the term RO_2 is used to include HO_2. The ratio of the rates at which reaction R3 and R2 proceed is given by equation ES5:

$$\frac{k_3 \cdot [RO_2]}{k_2 \cdot [NO]} \quad \text{(ES5)}$$

This ratio is equal to the ratio $\frac{P(PRP)}{P(O_3)+P(RONO_2)}$:

$$\frac{k_3 \cdot [RO_2]}{k_2 \cdot [NO]} = \frac{P(PRP)}{P(O_3)+P(RONO_2)} \quad \text{(ES6)}$$

The derivative of $\frac{k_3 \cdot [RO_2]}{k_2 \cdot [NO]}$ versus NO is:

$$\frac{\partial \left(\frac{k_3 \cdot [RO_2]}{k_2 \cdot [NO]}\right)}{\partial [NO]} = -\frac{\frac{k_3}{k_2}[RO_2]}{[NO]^2} \quad \text{(ES7)}$$

Hence the derivative of $\frac{P(PRP)}{P(O_3)+P(RONO_2)}$ versus [NO] is also given by the right term in Equation ES7.

Considering that for a given photochemical system $P(O_3)$ and $P(RONO_2)$ are related by $\frac{Y(O_3)}{Y(RONO_2)}$, the sum $P(O_3)$ + $P(RONO_2)$ can be expressed as:

$$P(O_3) + P(RONO_2) = P(O_3) + \frac{Y(RONO_2)}{Y(O_3)} \cdot P(O_3) \quad \text{(ES8)}$$

At constant contribution of HO_2 and other RO_2 radicals $\frac{Y(RONO_2)}{Y(O_3)}$ should be constant. If so, $P(O_3)$ may serve as a proxy for RO_2 consumption in reaction R2:

$$\frac{P(PRP)}{P(O_3)+P(RONO_2)} = \frac{P(PRP)}{\left(1+\frac{Y(RONO_2)}{Y(O_3)}\right)\cdot P(O_3)} \quad \text{(ES9)}$$

It thus follows that P(PRP) and $P(O_3)$ in dependence of [NO] is coupled according to:

$$-\frac{\partial\left(\frac{P(PRP)}{P(O_3)}\right)}{\partial[NO]} = \left(1+\frac{Y(RONO_2)}{Y(O_3)}\right)\cdot \frac{\frac{k_3}{k_2}\cdot[RO_2]}{[NO]^2} \quad \text{(ES10)}$$

Branching ratios as well as the rate constants k_3 and k_2 are determined by the peroxy radical *pattern.* The RO_2 pattern itself is controlled by the BVOC mixture, by [OH] and by [NO] . In particular contributions of HO_2 are important because $Y(RONO_2)$ is essentially zero for HO_2. For simplicity we assume that branching ratios and rate constants were constant from experiment to experiment because the same BVOC mixtures were added in all experiments. This assumption allowed to express the NO induced changes of the ratio $P(PRP)/P(O_3)$ by exchanging $\frac{k_3}{k_2}\cdot\left(1+\frac{Y(RONO_2)}{Y(O_3)}\right)$ by a constant (*const*):

$$-\frac{\partial\left(\frac{P(PRP)}{P(O_3)}\right)}{\partial[NO]} = const\cdot\frac{[RO_2]}{[NO]^2} \quad \text{(ES11)}$$

with *const* being a proportionality factor. The results of our experiments *a posteriori* verified the validity of the above given assumption.

In a photochemical system $\frac{P(PRP)}{P(O_3)}$ may change with varying $[NO]$ in a very complicated manner because variations of $[NO]$ should result in variations of [RO_2]. Here we distinguish two cases:

(1) The peroxy radical production rate, P(RO_2), stays constant independent of NO. In this case increasing [NO] should cause a decrease of [RO_2] and the power law dependence should show an exponent below -2.

(2) [RO_2] is independent of [NO] and nearly constant. It follows that $\frac{\partial\left(\frac{P(PRP)}{P(O_3)}\right)}{\partial[NO]} = const \cdot \frac{1}{[NO]^2}$ meaning that the ratio $\frac{P(PRP)}{P(O_3)}$ will change with varying [NO] in a way describable by power law dependence with an exponent of -2. One mechanism by which [RO_2] can stay constant and thus independent of [NO] is an increasing production rate of RO_2 P(RO_2) due to increasing steady state [OH].

S2: Determination of P(O_3)

Rates of photochemical ozone production, P(O_3), were determined considering the following source and loss terms for O_3.

Source terms for O_3:

a) Net addition to the chamber: $V \cdot \frac{\partial[O_3]}{\partial t} = F \cdot ([O_3]_{in} - [O_3])$ (ES12)

with V = volume of the chamber, F = air flow through the chamber, $[O_3]_{in}$= concentration of O_3 in the ingoing and $[O_3]$ = concentration of O_3 in the outgoing air stream. The reaction chamber was operated as continuously stirred tank reactor with air mixing rates much higher than exchange rates of air. Thus the ozone concentration measured at chamber outlet, $[O_3]$, is the average ozone concentration in the chamber. Note that in case of photochemical ozone formation $[O_3]$ will be higher than $[O_3]_{in}$. Process a) may switch from a source term to a loss term.

b) NO_2 photolysis: $V \cdot \frac{\partial[O_3]}{\partial t} = V \cdot J(NO_2) \cdot [NO_2]$ (ES13)

with J(NO_2) = rate of NO_2 photolysis and assuming that J(NO_2) limits the rate of process b) because the subsequent reaction: $O^3P + O_2 + M \rightarrow O_3 + M$ is much faster than NO_2 photolysis.

Loss terms for O_3:

c) Reactions with NO: $V \cdot \frac{\partial[O_3]}{\partial t} = -V \cdot k_1 \cdot [NO] \cdot [O_3]$ (ES14)

d) Ozone photolysis: $V \cdot \frac{\partial[O_3]}{\partial t} = -V \cdot J(O^1D) \cdot [O_3] \cdot f([H_2O])$ (ES15)

with $f([H_2O])$ = branching ratio of $O^1D + H_2O$ reactions over O^1D quenching to O^3P by O_2 and N_2 which leads to reformation of O_3.

e) Ozone reactions with BVOC: $V \cdot \frac{\partial[O_3]}{\partial t} = -V \cdot k_{BVOC} \cdot [O_3] \cdot [BVOC]$ (ES16)

with k_{BVOC} = average rate constant for BVOC + O_3 reactions.

f) Ozone reactions with OH: $V \cdot \frac{\partial[O_3]}{\partial t} = -V \cdot k_{OH} \cdot [O_3] \cdot [OH]$ (ES17)

with k_{OH} = rate constant of OH + O_3 reactions.

g) Ozone reactions with HO_2: $V \cdot \frac{\partial[O_3]}{\partial t} = -V \cdot k_{HO2} \cdot [O_3] \cdot [HO_2]$ (ES18)

with k_{HO2} = rate constant of HO_2 + O_3 reactions.

h) Wall losses: $V \cdot \frac{\partial[O_3]}{\partial t} = v^w \cdot A^w \cdot [O_3]$ (ES19)

with v^w = deposition velocity of ozone to the walls of the chamber with the wall area A^w.

Dominant source term is NO_2 photolysis, dominant loss term is reaction of O_3 with NO. If the system is in PSS, both rates are equal and cancel out. In the presence of VOC and OH, ozone production by NO_2 photolysis exceeds ozone losses in reactions with NO. The difference between (b) and (c) is attributed to reaction R2a and termed as ozone production rate:

$$P(O_3) = k_2 \cdot [NO] \cdot [RO_2] \cdot Y(O_3) \quad \text{(ES2)}$$

Under atmospheric conditions ozone losses due to ozone photolysis and reactions of O_3 with OH, HO_2, and BVOC are quite low and can be neglected for estimation of $P(O_3)$. In our reaction chamber the situation was different because $J(O^1D)$, [OH], [BVOC] and most probably also $[HO_2]$ were much higher than in the atmosphere. To calculate $P(O_3)$ therefore required consideration of ozone photolysis (d) and O_3 losses in processes *e* – *h*:

Ozone photolysis: The branching ratio of $O^1D + H_2O$ reactions in our chamber was: $f([H_2O]) \sim 0.09$ and ozone mixing ratios ranged between 46 and 85 ppb. At $J(O^1D) = 9\times10^{-4}$ s^{-1} photolytic ozone losses ranged between 13 and 24 ppb h^{-1}.

Compared to the high photolytic losses, ozone losses in processes *e* to *h* were of minor importance. The following loss rates (or upper limits of loss rates) were estimated:

e. Ozone losses in reactions with BVOC were estimated to be < 2 ppb h^{-1}:
BVOC concentrations in the reaction chamber were very low when the TUV lamp was on and OH reactions were dominant. In such cases concentrations of myrcene, (*E*)-β-ocimene exhibiting high reactivity towards OH were near to the detection limit or even below. These were also the BVOC with the highest reactivity towards O_3 and thus ozone losses due to these reactions were not reliably determinable. We therefore estimated an upper limit of O_3 losses assuming that a hypothetical BVOC with a high reactivity towards O_3 would be abundant at concentrations of 500 ppt. As rate constant $k_{BVOC} = 5.4\times10^{-16}$ cm^3 s^{-1} was used (= rate constant of O_3 + (*E*)-β-ocimene reactions, Atkinson, 1997).

f. Using $[OH] = 2.5\times10^7$ cm^{-3} (see Fig. 6 of the manuscript) and $k_{OH} = 7.3\times10^{-14}$ cm^3 s^{-1} (Sander et al., 2006) losses in OH reactions were estimated to ~0.4 ppb h^{-1}.

g. Assuming [HO_2] < 0.3 ppb (~ 8×10^9 cm^{-3}) as an upper limit for HO_2 concentrations (compare to Fig. S1) and using $k_{HO2} = 2\times10^{-15}$ cm^3 s^{-1} (Sander et al., 2006), O_3 losses in reactions with HO_2 were estimated to < 4 ppb h^{-1}.

h. As reported before (e.g. Neubert et al., 1993; Fares et al., 2008) wall losses in our chamber were very low. Less than 3% of the O_3 was lost within the residence time of the air in the reaction chamber (~ 63 min.) leading to an upper limit for ozone wall losses of < 2.6 ppb h^{-1}.

Compared to photolytic O_3 losses and losses due to higher O_3 concentrations in the outgoing air than in the ingoing air all the other losses (e-h) were low and therefore neglected.

The term of interest, $P(O_3) = k_2 \cdot [NO] \cdot [RO_2] \cdot Y(O_3)$, was determined after setting the differential equation for net ozone introduction, photochemical ozone production and ozone photolysis to steady state conditions resulting in Equation ES20:

$$P(O_3) = k_2 \cdot [NO] \cdot [RO_2] \cdot Y(O_3) = \frac{F}{V} \cdot ([O_3] - [O_3]_{in}) + J(O^1D) \cdot [O_3] \cdot f([H_2O]) \quad \text{(ES20)}$$

For comparison with J_7, $P(O_3)$ was determined for the point in time when new particle formation appeared. For the high $[NO_x]_0$ experiments $P(O_3)$ was thus measured 2 to 5 h after switching on the TUV lamp. For the low $[NO_x]_0$ experiments we used the data obtained about an hour after switching on the TUV lamp when $[O_3]$ was near to steady state.

S3: power law dependencies

To check for power law dependencies between J_7 and BNR and between $P(O_3)$ and BNR, respectively, logarithmic data of these data were plotted (Fig. S1).

As result we obtained a slope of: 2.3 ± 0.1, for the fit of ln(J_7) versus ln(BNR) indicating that J_7 increased approximately in a squared manner with increasing BNR. Considering that $[BVOC]_0$ was quite constant and at least did not vary systematically with $[NO_x]_0$, this indicates that J_7 decreased with increasing $[NO_x]_0$ in an approximately squared manner.

As result of the fit of ln($P(O_3)$) versus ln(BNR) we obtained -1.28 ± 0.3 indicating that $P(O_3)$ increased approximately linearly with decreasing BNR. Again, considering that $[BVOC]_0$ was

quite constant, this also indicated an approximately linear increase of $P(O_3)$ with increasing $[NO_x]_0$.

S4: determination of $[RO_2]$ from deviation from PSS

In a chemical system with photochemical O_3 formation $\frac{[NO_2]}{[NO]}$ is given by:

$$\frac{[NO_2]}{[NO]} = \frac{k_1 \cdot [O_3] + k_2 \cdot [RO_2]}{J(NO_2)} \quad \text{(ES21)}$$

The difference between measured $\frac{[NO_2]}{[NO]}$ and $\frac{[NO_2]}{[NO]}_{PSS}$ (Equation ES1) is: $\frac{k_2 \cdot [RO_2]}{J(NO_2)}$. The concentration of $[RO_2]$ can thus be estimated by using an average rate constant k_2. In two of our experiments it was possible to obtain data for $[RO_2]$ from observed deviation of $\frac{[NO_2]}{[NO]}$ from PSS. We used k_2 = 9×10^{-12} cm^3 s^{-1} (IUPAC, 2009) and $J(NO_2)$ = 4.3×10^{-3} s^{-1} as measured in the chamber with VOC free air and in the absence of O_3 photolysis by the TUV lamp.

Figure 9 of the manuscript shows the result obtained from the experiment with the highest NO_x addition (first row of Table 1 in the manuscript). Figure S2 shows the result of the second example where such estimation was possible (BNR = 3.2 ppbC/ppb, $[NO_x]_0$ = 39.4 ppb, [OH] increasing from 5.4×10^6 to 2.2×10^7 cm^{-3}, third row in Table 1 of the manuscript).

With respect to the temporal development of the photochemical system, the same result was obtained in both experiments. With proceeding photochemistry the deviation of observed $\frac{[NO_2]}{[NO]}$ from PSS increased, indicating that peroxy radical concentrations increased with time.

In the experiment shown in Figure S2, new particle formation became observable about 2 hours after starting OH production. At that time [NO] had decreased from ~9 ppb to ~0.85 ppb and estimated RO_2 concentrations had increased to ~200 ppt. In the experiment shown in Figure 9 of the manuscript NPF became observable about 5 hours after starting OH production. At that time [NO] had decreased from ~20 to ~1 ppb and estimated RO_2 concentrations had increased to ~ 300 ppt.

While absolute concentrations of [RO_2] depend critically on k_2, and therefore have large systematic errors, the relative comparison of [RO_2] for the two experiments is less error prone. In both experiments the chemical system, especially BVOC composition was similar. Thus also yields of organic nitrate formation should have been similar and similar RO_2 radicals should have been produced. Both make errors in k_2 less important for comparison.
We therefore concluded that [RO_2] was similar in both experiments. The observed difference in J_7 as measured in both experiments (J_7 = 0.46 cm^{-3} s^{-1} for [RO_2] ~ 200 ppt and J_7 = 0.02 cm^{-3} s^{-1} for [RO_2] ~ 300 ppt) shows that J_7 was not related to the concentrations of the bulk of first generation peroxy radicals.

S5: Estimation of [RO_2] for low NO_x conditions

As the squared relationship between J_7 and P(O_3) was valid in the whole range 1.1 < BNR < 10, it was necessary to compare [RO_2] for all these experiments. Because it was impossible to use deviation from PSS in the medium to low NO_x experiments, relative data were determined. Reference case was the experiment with the highest $[NO_x]_0$ addition (Figure 9 in the manuscript).
Relative RO_2 concentrations were estimated assuming steady state conditions for peroxy radicals: Due to the high reactivity the lifetime of peroxy radicals is on the order of seconds. This is very short compared to the temporal changes of [OH], [O_3], [NO] in the chamber (see Figs. 4 and 9 in the manuscript and Fig. S2). As production and loss rates changed on time scales of hours, assumption of steady state conditions for [RO_2] was justified. This assumption allowed expressing [RO_2] as ratio of RO_2 production rates P(RO_2) over a loss rate L(RO_2):

$$[RO_2] = \frac{P(RO_2)}{L(RO_2)} \quad \text{(ES22)}$$

with

$$L(RO_2) = k_2 \cdot [NO] + k_3 \cdot [RO_2] \quad \text{(ES23)}$$

At the conditions in the chamber, BVOC oxidation was dominated by OH reactions. Thus $P(RO_2)$ could be written as:

$$P(RO_2) = [BVOC] \cdot [OH] \cdot k_4 \cdot Y(RO_2) \quad \text{(ES24)}$$

In Equation ES24, k_4 is an average rate constant for BVOC + OH reactions and $Y(RO_2)$ is the yield of peroxy radical formation from the BVOC mix. The BVOC mixtures during the respective experiments were similar. Therefore also k_4 and $Y(RO_2)$ were similar allowing expressing the ratio of peroxy radical production rates P(PRP) according to Equation ES25.

$$\frac{P(RO_2)_R}{P(RO_2)_D} = \frac{[OH]_R \cdot [BVOC]_{0,R}}{[OH]_D \cdot [BVOC]_{0,D}} \quad \text{(ES25)}$$

In Equation ES25, the index R represents the reference case, and the index D represents the data set for which $[RO_2]$ had to be determined. In all calculations we used [OH] as measured during the onset of new particle formation. For the low NO_x experiments these were the OH concentrations measured during the first hour of the experiments (see Table 1 in the manuscript). For the high NO_x experiments these were the OH concentrations measured 2 – 5 h after the TUV lamp was switched on.

The ratio of RO_2 concentrations could be written as:

$$\frac{[RO_2]_D}{[RO_2]_R} = \frac{P(RO_2)_D \cdot ([k_2 \cdot [NO]_R + k_3 \cdot [RO_2]_R)}{P(RO_2)_R \cdot ([k_2 \cdot [NO]_D + k_3 \cdot [RO_2]_D)} \quad \text{(ES26)}$$

Rearrangement of Equation ES26 leads to Equation ES27:

$$[RO_2]_D^2 + [RO_2]_D \cdot \frac{k_2}{k_3}[NO]_D - \frac{P(RO_2)_D}{P(RO_2)_R} \cdot [RO_2]_R \cdot \left(\frac{k_2}{k_3}[NO]_R + [RO_2]_R\right) = 0 \quad \text{(ES27)}$$

$[RO_2]_R$ was ~300 ppt (see Figure 9 in the manuscript), and $[OH]_R$ was ~ 2.6×10^7 cm^{-3} (see red square in Fig. 6 of the manuscript). $[OH]_D$ was measured and k_2 was set to 9×10^{-12} cm^3 s^{-1} (IUPAC, 2009) i. e. identical to the value used in the estimations of $[RO_2]$ from deviation from PSS.

Most uncertain quantities in Equation ES27 were $[NO]_D$ and k_3. Thus, we used upper and lower limits for each of these quantities. As upper limit for $[NO]_D$ the NO concentration estimated for PSS from the measured [NO_x] and [O_3] was used. As lower limit, $[NO]_D$was set to zero.

To estimate an upper limit for k_3, it was assumed that [HO_2] contributed to 90 % to [RO_2]; to estimate a lower limit for k_3, it was assumed that [HO_2] contributed to 10 % to [RO_2]. As can be seen from data given in the master chemical mechanism (MCM) for monoterpenes, rate constants for reactions of first generation RO_2 radicals with HO_2 are much higher than those of other RO_2 –R'O_2 reactions ($RO_2 + HO_2 \sim 3.1\times10^{-11}$ cm^3 s^{-1}, $RO_2 + R'O_2 \sim 6.5\times10^{-15} – 8.8\times10^{-13}$ cm^3 s^{-1}). This allows neglecting RO_2+R'O_2 reactions as important loss terms for peroxy radicals. The relative abundance of HO_2 in the RO_2 mix is the main determining factor for RO_2 loss rates at low NO_x conditions. We therefore assumed $k_3 = 2.8\times10^{-11}$ cm^3 s^{-1} (for [HO_2] ~ 90% of [RO_2]) to be an upper limit for k_3 and $k_3 = 3.1\times10^{-12}$ cm^3 s^{-1} (for [HO_2] ~ 10% of [RO_2]) to be a lower limit for k_3.

Table S1 lists [RO_2] estimated for the three combinations: $k_3 = 2.8\times10^{-11}$ cm^3 s^{-1} and $[NO]_D$from PSS termed as $[RO_2]^a_{rel}$, $k_3 = 3.1\times10^{-12}$ cm^3 s^{-1} and $[NO]_D$from PSS termed as $[RO_2]^b_{rel}$, and for $k_3 = 2.8\times10^{-11}$ cm^3 s^{-1} and $[NO]_D = 0$ termed as $[RO_2]^c_{rel}$. As obvious from Equation ES27 the fourth of the possible combinations: $k_3 = 3.1\times10^{-12}$ cm^3 s^{-1} and $[NO]_D = 0$ gives the same result as $[RO_2]^c_{rel}$ because k_3 cancels out. For better comparison, Table S1 also lists the range of minimum and maximum relative [RO_2] compared to the reference case (~ 300 ppt).

Comparing maximum and minimum values for [RO_2] for individual experiments it is obvious that the data differ by roughly a factor of two. Hence the uncertainty in [RO_2] caused by the uncertainties in k_3 and in [NO] had no substantial impact on results for individual experiments. As the variations of $[NO]_D$ and k_3 were quite large, we believe that the estimations on the ranges of relative [RO_2] are realistic.

Comparing relative RO_2 concentrations between experiments starting at high $[NO_x]_0$ conditions and at low $[NO_x]_0$, respectively, it is obvious that also these numbers show variability of roughly a factor of 2. Independent of the combination of k_3 and [NO] used for the estimations there was no systematic variation from high to low NO_x experiments (compare numbers in columns).

Again, we put not too much attention to the absolute numbers. But the photochemical systems were very similar from experiment to experiment allowing reliable comparison between experiments. We therefore concluded that $[RO_2]$ at the onset of NPF was quite constant in all experiments. Contrary, J_7 varied by 3 orders of magnitude over the whole BNR range. In the range 1.1 < BNR < 10 where comparison of J_7 and $P(O_3)$ was possible J_7 still varied by 2 orders of magnitude allowing the conclusion that J_7 was not related to P(PRP).

S6 Sensitivity tests and general considerations

Based on the similarity of $[RO_2]$ estimated for the high and low $[NO_x]_0$ experiments, respectively, we conclude that production rates of first generation PRP were not the rate limiting step for NPF. We further test the validity of this conclusion with the following hypothesis. We assume that first permutation reactions of first generation RO_2 radicals are the rate limiting step for NPF and estimate how high $[RO_2]$ should have been in that case during the low $[NO_x]_0$ experiments:

If reaction R3 is the rate limiting step in new particle formation, J_7 should be proportional to the rate of reaction R3:

$$J_7 = x \cdot k_3 \cdot [RO_2] \cdot [RO_2] \quad \text{(ES28)}$$

with x = a proportionality factor.

As base we again use the high NO_x experiment as shown in Fig. 9 of the manuscript. When particle formation started, RO_2 was estimated to be around 300 ppt and J_7 was in the range of 0.13 cm^{-3} s^{-1}. As typical value for J_7 at low NO_x conditions we use J_7 = 66 cm^{-3} s^{-1} (average of J_7 without NO_x addition, see Table 1 in the manuscript). Assuming the proportionality factor *x* to be constant would mean that threshold RO_2 concentrations should increase with the square root of J_7. Using J_7 = 66 cm^{-3} s^{-1} leads to a threshold RO_2 concentration of 6.8 ppb.

Assuming that the dependence of J_7 on $[RO_2]$ would be to power law of 1.6 instead of 2 would lead to even higher $[RO_2]$ of 49 ppb.

Both values for $[RO_2]$, 6.8 and 49 ppb are unrealistic high even when considering that the absolute numbers for RO_2 as shown in Fig. 9 may be an order of magnitude too high. The strong variations in J_7 cannot at all be explained by variations of $[RO_2]$.

From our estimations in sections S4 to S6 we conclude that permutation reactions of first generation RO_2 radicals cannot be the rate limiting step for new particle formation.

S7 Determination of J_7 and estimation of uncertainty limits for J_7

Determining rates of new particle formation (J_7) from chamber data requires consideration of wall losses and of background particles. Both may skew determinations of J_7 if their impact on J_7 is substantial.

We used BVOC concentrations around 10 ppb and, as also found in other studies (e.g. Mentel et al., 2009, Mentel et al., 2013), formation of new particles from ozonolysis alone was low as long as BVOC concentrations in that range were applied. Therefore also the background particle number concentration formed from ozonolysis of α-pinene and from the OH formed during ozonolysis was low. Without NO_x addition the particle number concentration (P_N) of the background ranged between 100 cm^{-3} and 300 cm^{-3}. Background P_N was quite constant during individual experiments with fluctuations < 10 %. Inducing NPF by OH formation (TUV lamp on) increased P_N to ~3×10^4 cm^{-3} (see Fig. 3 in the manuscript, red trace). Since the maximum P_N was much higher than fluctuations of background number concentrations, J_7 was not substantially skewed by background particles, since it was determined from the slope of P_N versus time .

NO_x addition to the chemical system decreased J_7 as well as the background particle numbers. At $[NO_X] \geq 40$ ppb, background P_N were between 3 cm^{-3} and 7 cm^{-3} and fluctuated from ~1 cm^{-3} to ~11 cm^{-3}. Compared to the maximum P_N determined during NPF events at $[NO_x] \geq 40$ ppb (130 - 2200 cm^{-3}) these fluctuations are still small. Assuming that no particles were introduced into the chamber and all background particles were produced in the chamber, we estimate the upper limit of 7 nm particles formed as background using the maximum particle number of 11 cm^{-3} and the residence time of the air in the chamber (63 min). This results in max. background J_7 ~ 0.0032 cm^{-3} s^{-1}. This is by far lower than the lowest J_7 determined during our experiments. Considering this as worst case estimation, we assess possible errors in J_7 determinations due to background particles as low over the whole range of applied NO_X.

To estimate the impacts of wall losses on J_7 the following experiment was conducted using two different CPCs in parallel. One was a TSI 3022A with a cut off diameter of 7 nm, the other one was a TSI 3786 coupled to a particle size magnifier (PSM, Airmodus A09) with a nominal cut-off diameter of 1.5 nm for the PSM/CPC system. Ten ppb α-pinene and 80 ppb

O_3 were added to the chamber (without NO_X addition). Before starting the photolytic production of OH radicals, the system was in steady state showing stable number concentrations around 130 cm^{-3} particles > 1.5 nm and ~11 cm^{-3} for particles with diameters > 7 nm. Short after photolytic production of OH radicals, P_N measured by the PSM increased rapidly to ~1500 cm^{-3} within about 1.5 minutes. Then the OH production was switched off and P_N as measured with the PSM decreased exponentially indicating a first order loss process (loss coefficient - 0.0017 ± 0.0001 s^{-1}, R^2 = 0.9, τ = 9.8 min.). P_N as measured with the 7 nm CPC stayed constant at ~11 over the whole measurement period proving that particles with diameters > 7 nm did not substantially contribute to P_N during that experiment. From this we conclude that the exponential decay observed for the number concentration of particles with diameters between 1.5 and 7 nm was mainly due to wall losses of small particles. The loss coefficient of 0.0017 s^{-1}, equivalent to a lifetime of about 10 minutes, indicated that wall losses in our chamber had substantial impact on the observation of formation rates of new particles.

To consider the impacts of wall losses, J_7 was determined in the following manner. It was assumed that new particle formation and wall losses were the dominant processes and that impacts of outflow and coagulation on P_N were negligible. This led to the approach:

$$J_7 = \frac{\partial(P_N)}{\partial t} + L(P_N) \qquad \text{(ES29)}$$

In equation ES29, $\frac{\partial(P_N)}{\partial t}$ is the first derivative of the measured P_N as a function of time at the inflection point. $L(P_N)$ is the loss rate and calculated as product of loss coefficient and P_N at the respective inflection points.

Depending on the experiment the contributions of $\frac{\partial(P_N)}{\partial t}$ and $L(P_N)$ to J_7 were different. At high $\frac{\partial(P_N)}{\partial t}$, $L(P_N)$ and $\frac{\partial(P_N)}{\partial t}$ were similar in magnitude indicating that even at the fastest temporal increases of P_N, J_7 was already affected by wall losses. At the lowest measured $\frac{\partial(P_N)}{\partial t}$, $L(P_N)$ exceeded $\frac{\partial(P_N)}{\partial t}$ by a factor of 6 indicating that for small $\frac{\partial(P_N)}{\partial t}$ the loss rates dominate $\frac{\partial(P_N)}{\partial t}$. Hence, the uncertainty of wall losses determines the error in J_7. Therefore different wall losses were used to calculate uncertainty limits for J_7. We estimated the uncertainty limits for J_7 by doubling and halving the measured loss coefficient, respectively. The upper limit was estimated using a loss coefficient of 0.0034 s^{-1} corresponding to a

lifetime of 5 minutes. The lower limit for J_7 was estimated using a loss coefficient of 0.00085 s^{-1} corresponding to a lifetime of 20 minutes.

References to supplemental information

Atkinson, R.: Gas-phase tropospheric chemistry of volatile organic compounds: 1. Alkanes and alkenes. J. Phys. Chem. Reference Data, 26, (2), 215-290, 1997.

Fares, S., Loreto, F., Kleist, E., and Wildt, J.: Stomatal uptake and stomatal deposition of ozone in isoprene and monoterpene emitting plants. Plant Biology, 10, 44 – 54, 2008.

Hallquist, M., Wenger, J. C., Baltensperger, U., Rudich, Y., Simpson, D., Claeys, M., Dommen, J., Donahue, N. M., George, C., Goldstein A. H., Hamilton J. F., Herrmann, H., Hoffmann, T., Iinuma, Y., Jang M., Jenkin M. E., Jimenez, J. L., Kiendler-Scharr, A., Maenhaut, W., McFiggans, G., Mentel Th. F., Monod A., Prévôt, A. S. H., Seinfeld, J. H., Surratt, J. D., Szmigielski R., and Wildt, J.: The formation, properties and impact of secondary organic aerosol: current and emerging issues. Atmos. Chem. Phys., 9, 5155–5236, 2009.

IUPAC Subcommittee for Gas Kinetic Data Evaluation, http://www.iupac-kinetic.ch.cam.ac.uk/, 2009.

Leighton, P. A.: Photochemistry of Air Pollution. Academic Press, San Diego, CA, USA, 1961.

Master Chemical Mechanism, MCM: http://mcm.leeds.ac.uk/MCM/roots.htt

Mentel, Th. F., Wildt, J., Kiendler-Scharr, A., Kleist, E., Tillmann, R., Dal Maso, M., Fisseha, R., Hohaus, Th., Spahn, H., Uerlings, R., Wegener, R., Griffiths, P. T., Dinar, E., Rudich, Y., and Wahner, A.: Photochemical production of aerosols from real plant emissions, Atmos. Chem. Phys., 9, 4387–4406, doi:10.5194/acp-9-4387-2009, 2009.

Mentel, Th. F., Kleist, E., Andres, S., Dal Maso, M., Hohaus, T., Kiendler-Scharr, A., Rudich, Y., Springer, M., Tillmann, R., Uerlings, R., Wahner, A., and Wildt, J.: Secondary aerosol formation from stress-induced biogenic emissions and possible climate feedbacks, Atmos. Chem. Phys., 13, 8755–8770, doi:10.5194/acp-13-8755-2013, 2013.

Neubert, A., Kley, D., Wildt, J., Segschneider, H. J., and Förstel, H.: Uptake of NO, NO_2 and O_3 by sunflower and tobacco: dependence on stomatal conductivity. Atmos. Environm. 27A, 2137-2145, 1993.

Sander, S. P., Friedl, R. R., Golden, D. M., Kurylo, M. J., Moortgat, G. K., Keller-Rudek, H., Wine P. H., Ravishankara, A. R., Kolb , C. E., Molina, M. J., Finlayson-Pitts, B. J., Huie, R. E., and Orkin, V. L.: Chemical Kinetics and Photochemical Data for Use in

Atmospheric Studies, Evaluation Number 15, JPL Publication 06-2, http://jpldataeval.jpl.nasa.gov/, 2006.

Table S1: Results from estimations of relative peroxy radical concentrations. Data for $[RO_2]$ obtained for the experiment at BNR = 1.1 were taken as reference.

$[RO_2]^a_{rel}$: k_3 = 2.8×10^{-11} cm^3 s^{-1}, $[NO]_D$ from PSS,

$[RO_2]^b_{rel}$: k_3 = 3.1×10^{-12} cm^3 s^{-1}, $[NO]_D$ from PSS,

$[RO_2]^{c,d}_{rel}$: k_3 = 2.8×10^{-11}/3.1×10^{-12} cm^3 s^{-1}, $[NO]_D$ = 0.

The last column lists the minimum and maximum $[RO_2]$ compared to 300 ppt, i.e. the reference case.

BNR [ppbC]/[ppb]	$[BVOC]_0$ [ppbC]	[OH] [cm^{-3}] ×10^7	$[RO_2]_{PSS}$ [ppt]	$[RO_2]^a_{rel}$ [ppt]	$[RO_2]^b_{rel}$ [ppt]	$[RO_2]^{c,d}_{rel}$ [ppt]	Range %
1.1	119	2.58	300	-	-	-	-
1.8	122	2.50	#	169	150	299	50 – 100
3.2	124.5	2.20	200	164	136	283	45 – 94
4.3	98.5	*	--	*	*	*	*
8.9	109.5	1.68	--	149	95	232	31 – 77
10.2	104.3	1.89	--	164	102	240	34 – 80
12.8	105	*	--	*	*	*	*
14.4	106.3	1.91	--	181	115	244	38 – 81
18.0	88.3	1.83	--	168	98	218	33 – 73
24.4	79.8	1.71	--	162	91	200	30 – 67
25.4	124.5	1.47	--	183	111	232	37 – 77
28.6	117	1.71	--	200	124	242	41 – 81
29.8	97.5	1.68	--	182	108	219	36 – 73
61.1	100	1.40	--	181	112	203	37 – 68
62.0	101.5	*	--	*	*	*	*
79.2	129.5	0.99	--	172	104	194	35 – 65
255.8	76.8	*	--	*	*	*	*
277.5	83.3	1.58	--	192	164	196	54 – 65
300.0	90	1.59	--	201	172	205	57 – 68
326.7	98	1.06	--	170	140	175	47 – 58
329.2	98.8	*	--	*	*	*	*
345.8	103.8	1.16	--	183	155	188	51 – 63
363.8	109	*	--	*	*	*	*
412.5	124	*	--	*	*	*	*
414.2	124.3	1.11	--	197	168	201	56 - 67
415.0	124.5	*	--	*	*	*	*

-- [NO] too low to allow reliably determination of deviation from PSS

no $[RO_2]_{PSS}$ due to failure of NO_x analytics

* no data due to failure of OH measurement

Figure S1

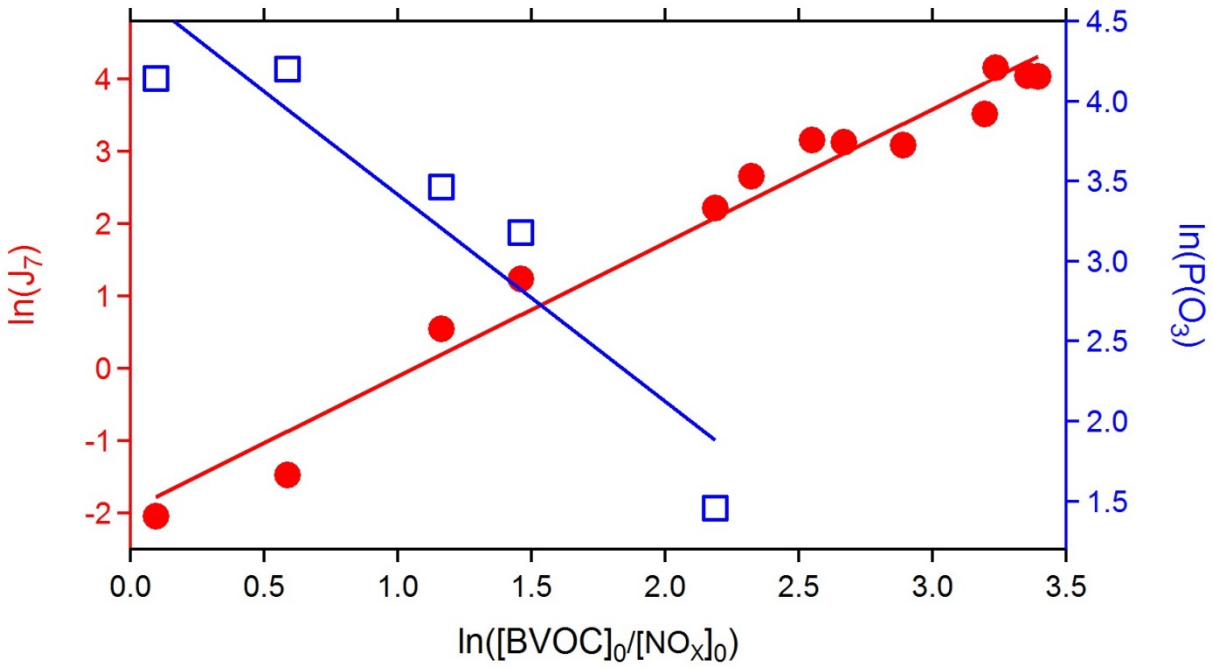

Fig. S1: double logarithmic plots of J_7 versus BNR (left scale, red circles) and of $P(O_3)$ versus BNR (blue squares, right scale). The red and blue lines show the results from the respective least square fits. Data used for the fit of $ln(J_7)$ versus ln(BNR) were restricted to data points where impacts of NO_x were obvious (BNR < 30 [ppbC]/[ppb]). Data used for the fit of $ln(P(O_3)$ versus ln(BNR) were restricted to reliable data for $P(O_3)$ ($P(O_3)$ > 2.5 ppb h^{-1}). Note the different scales at both y-axes.

Figure S2

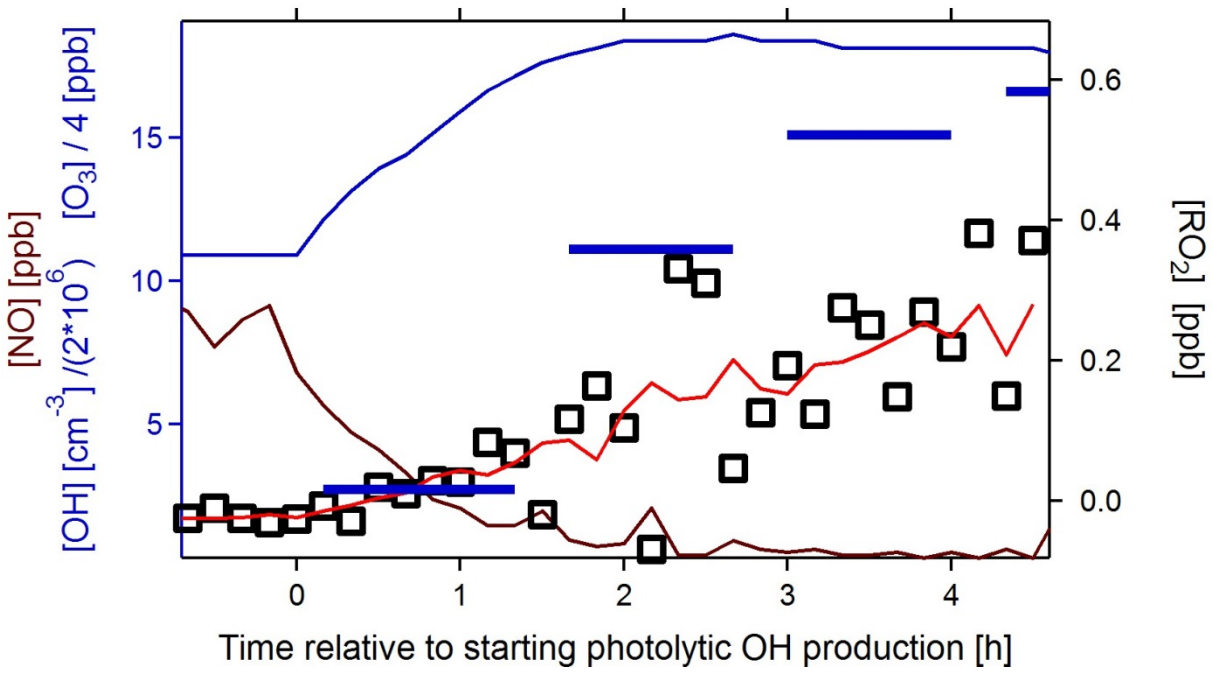

Fig. S2: Estimated $[RO_2]$ ($= \sum[RO_2^i]$) using deviation from PSS and an average rate constant k_2 = 9×10^{-12} cm^3 s^{-1} for reaction R2. The open squares (right hand y-scale) show the original data; the red line shows the five point moving average of the [RO_2] data (right hand y-scale). The brown line shows NO concentrations measured during that experiment, the blue bars show OH concentrations divided by 2×10^6 for clarity, and the blue line shows the ozone concentrations divided by 4 for clarity (all data on left hand y-scale). New particle formation started about 2 h after the TUV lamp was switched on. At that point in time [NO] had decreased to ~ 0.8 ppb and [RO_2] had increased to ~ 200 ppt.